

Pt^{II}-Catalyzed Ethylene Hydrophenylation: Influence of Dipyridyl Chelate Ring Size on Catalyst Activity and Longevity

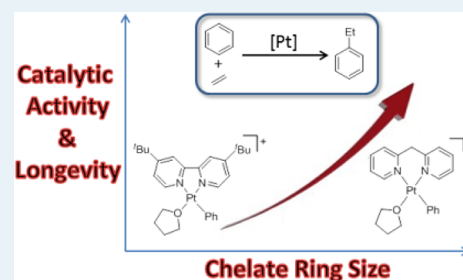
Bradley A. McKeown,[†] Hector Emanuel Gonzalez,[‡] T. Brent Gunnoe,^{*,†} Thomas R. Cundari,^{*,‡} and Michal Sabat[†]

[†]Department of Chemistry, University of Virginia, Charlottesville, Virginia 22904, United States

[‡]Center for Advanced Scientific Computing and Modeling, Department of Chemistry, University of North Texas, Denton, Texas 76203, United States

S Supporting Information

ABSTRACT: Expansion of the dipyridyl ligand from a five- to six-membered chelate for Pt^{II}-catalyzed ethylene hydrophenylation provides an enhancement of catalyst activity and longevity. Mechanistic studies of [(dpm)Pt(Ph)(THF)]⁺[BAR'₄]⁻ [dpm = 2,2'-dipyridylmethane, and Ar' = 3,5-(CF₃)₂C₆H₃] attribute the improved catalytic performance at elevated temperatures to a favorable change in entropy of activation with an increase in chelate ring size. The Pt^{II} catalyst precursor [(dpm)Pt(Ph)(THF)]⁺[BAR'₄]⁻ is among the most active catalysts for ethylene hydrophenylation by a non-acid-catalyzed mechanism.



KEYWORDS: C–H activation, platinum, aromatic alkylation, olefin hydroarylation, mechanism

INTRODUCTION

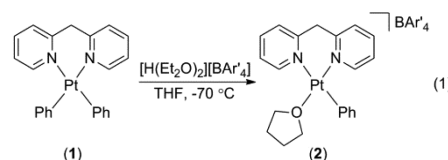
Synthesis of alkyl arenes from arenes and olefins has historically been achieved using Lewis acid catalysts.¹ Transition metal catalysts that operate via the insertion of olefin into metal–aryl bonds and subsequent metal-mediated aromatic C–H activation offer opportunities for improvement over acid-catalyzed processes.² For example, transition metal-mediated pathways could reduce the level of polyalkylation, bias reactions with α -olefins toward anti-Markovnikov products, regioselectively produce dialkyl arenes (e.g., 1,2-, 1,3-, or 1,4-dialkyl benzenes) from monoalkyl arenes, and catalyze oxidative olefin hydroarylation to directly produce vinyl arenes.^{2b,c} Until recently, transition metal-catalyzed olefin hydroarylation has been limited to the use of chelate-assisted or activated substrates.^{2a,3} Catalysts based on Ir, Ru, and Pt have been reported with unactivated substrates (e.g., benzene and ethylene).^{2c,d,4} However, these systems have yet to achieve levels of selectivity and activity sufficient for application to fine or commodity chemical synthesis, and detailed studies of the impact of the catalyst's steric and electronic profile on activity and/or selectivity are needed for the rational design of improved catalysts.

Previously, we reported a study of ethylene hydrophenylation catalyzed by [(^tbpy)Pt(Ph)(THF)]⁺[BAR'₄]⁻ [^tbpy = 4,4'-di-*tert*-butyl-2,2'-bipyridine, and Ar' = 3,5-(CF₃)₂C₆H₃] and proposed a catalytic cycle that incorporates both ethylene insertion and benzene C–H bond activation.^{4b} Puddephatt et al. have shown that ^tbpy and 2,2'-dipyridylmethane (dpm) have nearly identical donor abilities when coordinated to Pt^{II}, as determined from a comparison of carbonyl stretching frequencies of [(N~N)Pt(CO)(Me)]⁺ model complexes

(N~N = ^tbpy or dpm).⁵ Thus, the effect of chelate ring size on bis(pyridyl) Pt^{II}-catalyzed ethylene hydrophenylation can be directly evaluated without a substantial change in metal electron density by substituting ^tbpy with dpm. Herein, we report that substituting the ^tbpy ligand of [(^tbpy)Pt(Ph)(THF)]⁺ with dpm provides a more active (at ≥ 90 °C) and longer-lived catalyst. In fact, [(dpm)Pt(Ph)(THF)]⁺[BAR'₄]⁻ (**2**) is among the most active and longest-lived catalysts for ethylene hydrophenylation by a non-acid-catalyzed process. Mechanistic studies suggest that the different activities of the ^tbpy- and dpm-supported catalysts are largely a result of entropic factors.

RESULTS AND DISCUSSION

Complex **2** was prepared by protonation of (dpm)Pt(Ph)₂ (**1**) with [H(Et₂O)₂][BAR'₄] at -70 °C in THF (eq 1). Catalytic ethylene hydrophenylation using **2** was evaluated, and the results are summarized in Table 1.



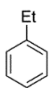
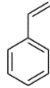
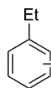
At 100 °C under 0.1 MPa of ethylene, a solution of 0.01 mol % **2** (relative to benzene) results in 55.3 turnovers (TO) of ethylbenzene, 10.6 TO of diethylbenzenes, and trace quantities

Received: March 26, 2013

Revised: April 15, 2013

Published: May 3, 2013

Table 1. Catalytic Ethylene Hydrophenylation Using **2**^a

Temperature (°C)				<i>o:m:p</i> ^b	TOF ^c (10 ⁻³ s ⁻¹)
90	16.8 ^d	0.0	4.0	1:12:8	1.4
	(74.7) ^e	(0.2)	(26.6)		
100	55.3	0.4	10.6	1:10:7	4.6
	(194.9)	(1.1)	(39.2)		
110	199.2	0.6	40.5	1:30:20	16.7
	(252.8)	(0.9)	(53.5)		
120	211.9	1.2	44.5	1:32:22	17.9
	(233.3)	(1.5)	(50.7)		
	[244.5]	[1.7]	[54.5]		

^aAt 0.01 mol % catalyst in C₆H₆ with 0.1 MPa of C₂H₄ and hexamethylbenzene (HMB) as an internal standard. ^bRatio of 1,2-, 1,3-, and 1,4-diethylbenzene after 4 h. ^cTurnover frequency calculated on the basis of the total number of turnovers after 4 h. ^dTurnovers after 4 h as determined by GC/MS. ^eNumbers in parentheses are turnovers after 16 h. ^fNumbers in brackets are turnovers after 36 h.

of styrene after 4 h, corresponding to a turnover frequency (TOF) of $4.6 \times 10^{-3} \text{ s}^{-1}$ (the formation of diethylbenzene is counted as a single catalytic TO). At ≤ 100 °C, plots of TO versus time reveal minimal catalyst deactivation after 4 h (Figures 1 and 2). Prolonged reaction times gave 235.2 and 364.4 total TO of alkyl benzenes after 16 and 36 h, respectively. A final turnover number (TON) after 110 h at 100 °C is 469.

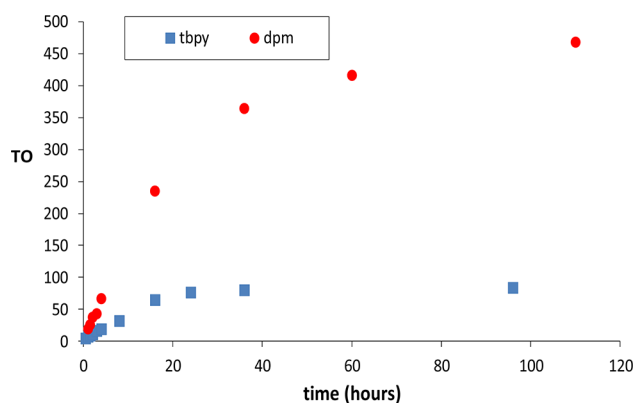


Figure 1. Comparison of TO vs time for ethylene hydrophenylation (100 °C) catalyzed by [(N~N)Pt(Ph)(THF)]⁺ [N~N = tppy (squares) or dpm (circles)]. At 0.01 mol % Pt in C₆H₆ with 0.1 MPa of C₂H₄ and HMB as an internal standard.

The influence of temperature on catalyst activity and stability was evaluated. At 90 °C under 0.1 MPa of ethylene pressure, a solution of **2** in benzene results in a TOF of $1.4 \times 10^{-3} \text{ s}^{-1}$ (calculated after 4 h). Thus, increasing the temperature to 100 and 110 °C increases the rate of ethylene hydrophenylation compared to the rate of the reaction at 90 °C by factors of ~ 3 and ~ 17 , respectively; however, catalyst deactivation becomes more competitive at elevated temperatures. The TON values after 36 h at 110 °C (~ 331) and 120 °C (~ 301) are lower than that observed at 100 °C (~ 364).

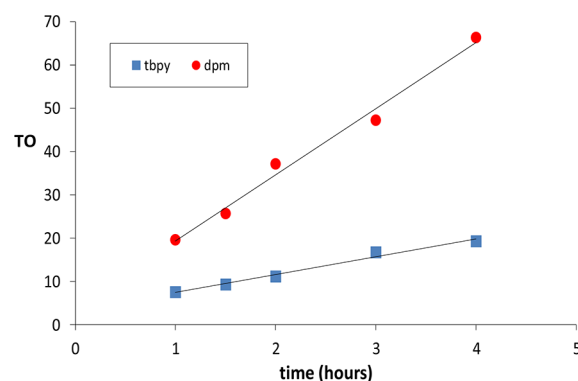


Figure 2. Comparison of TO vs time (≤ 4 h) for ethylene hydrophenylation (100 °C) catalyzed by [(N~N)Pt(Ph)(THF)]⁺ [for N~N = tppy (squares), $R^2 = 0.98$; for N~N = dpm (circles), $R^2 = 0.99$]. At 0.01 mol % Pt in C₆H₆ with 0.1 MPa of C₂H₄ and HMB as an internal standard.

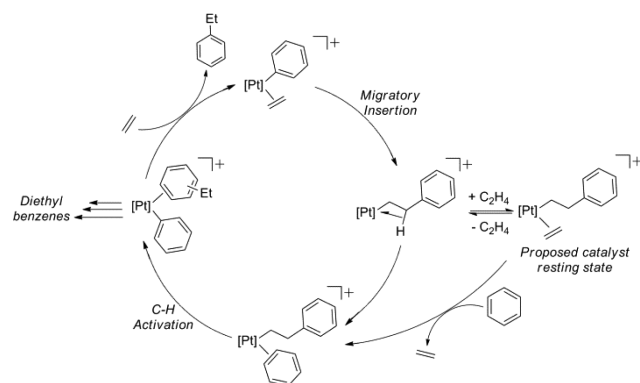
To compare the rate of catalytic ethylene hydrophenylation between **2** and [(tppy)Pt(Ph)(THF)][BAR'₄] (**3**), we used TOFs calculated after reaction for 4 h, which show that **2** catalyzes ethylene hydrophenylation ~ 3.5 times faster than **3** at 100 °C.^{4b} For example, catalysis at 100 °C under 0.1 MPa of ethylene pressure with [(tppy)Pt(Ph)(THF)]⁺ exhibits a TOF of $1.3(2) \times 10^{-3} \text{ s}^{-1}$ after 4 h, while a TOF of $4.6(8) \times 10^{-3} \text{ s}^{-1}$ was observed for **2**. We selected the 4 h time point because TO versus time plots reveal little evidence of catalyst deactivation (Figures 1 and 2). The linear regression in Figure 2 does not extrapolate through the origin because of the heating period required to bring the reaction solutions to 100 °C.

At 100 °C with 0.1 MPa of ethylene, almost complete catalyst deactivation is observed after 24 h for **3**, but **2** remains active over a period of more than 4 days (Figure 1). Monitoring catalysis using **2** until deactivation results in a TON of 469, which is an ~ 5.6 -fold increase compared to that with the tppy catalyst (TON of 84) under identical conditions. The identity of the catalyst decomposition product is unknown as a black material (presumably Pt black) and several intractable products are observed by ¹H NMR spectroscopy at the end of the reaction. Using plots of TOF versus time, we modeled catalyst deactivation kinetically. Both complex **2** and **3** display kinetics that are best modeled by a process that is second-order in platinum complex concentration.

Our proposed mechanism for cationic Pt^{II}-catalyzed ethylene hydrophenylation, based on detailed studies of **3**, is summarized in Scheme 1.^{4b} Substitution of the THF ligand with ethylene initiates the cycle, followed by the insertion of ethylene into the Pt–Ph bond. After insertion, an additional 1 equiv of ethylene coordinates to form the catalyst resting state [(N~N)Pt-(CH₂CH₂Ph)(η^2 -C₂H₄)]⁺ [N~N = dpm (**4**) or tppy (**5**)], which has been observed during catalysis by ¹H NMR spectroscopy for both **2** and **3**. Mechanistic studies could not differentiate between reaction pathways in which the resting state is incorporated into or removed from the catalytic cycle.^{4b} Displacement of ethylene by benzene and rate-limiting C–H activation result in the formation of [(N~N)Pt(η^2 -C₆H₅Et)(Ph)]⁺. Calculations for the tppy–Pt complex suggest that benzene C–H bond activation occurs by oxidative addition to form a Pt^{IV} intermediate.^{4b} Ethylbenzene is liberated by substitution with ethylene.

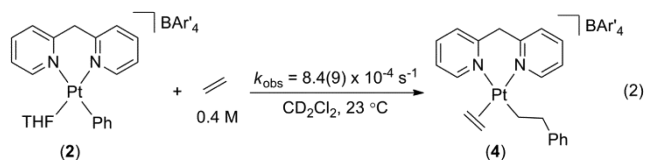
In an effort to explain the difference in catalytic activity between **2** and **3**, the insertion of ethylene into the Pt–Ph bond

Scheme 1. Proposed Catalytic Cycle for Cationic Pt^{II}-Catalyzed Ethylene Hydrophenylation^a



^a[Pt] = (bpy)Pt or (dpm)Pt.

and benzene C–H bond activation were probed individually for complex **2**. Ethylene readily inserts into the Pt–Ph bond of **2** to form [(dpm)Pt(CH₂CH₂Ph)(η²-C₂H₄)] [BAr'₄] (**4**). Under pseudo-first-order conditions, the conversion of **2** to **4** in CD₂Cl₂ at 23 °C in the presence of 0.4 M C₂H₄ proceeds with an observed rate constant of 8.4(9) × 10⁻⁴ s⁻¹ (eq 2). Thus, the observed rate of ethylene insertion for **2** is slower than that of [(bpy)Pt(Ph)(THF)]⁺ (**3**) (*k*_{obs} = 1.46 × 10⁻³ s⁻¹) under similar conditions by a factor of ~1.7.^{4b}



The structure of **4** is shown in Figure 3. As observed for the structure of [(bpy)Pt(CH₂CH₂Ph)(η²-C₂H₄)]⁺ (**5**),^{4b} the

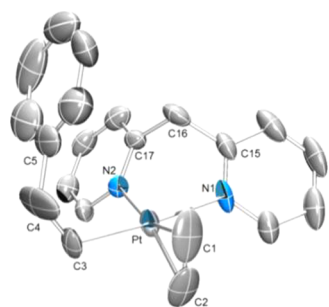
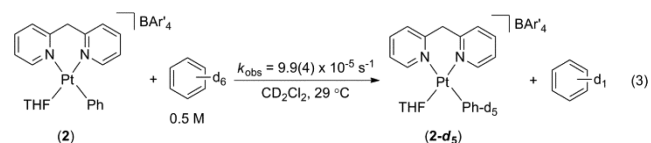


Figure 3. ORTEP diagram of [(dpm)Pt(CH₂CH₂Ph)(η²-C₂H₄)] [BAr'₄] (**4**) (50% probability; H atoms and BAr'₄ anion omitted for the sake of clarity). Selected bond lengths (in angstroms): Pt–N1, 2.135(7); Pt–N2, 2.068(6); Pt–C3, 2.049(8); Pt–C1, 2.113(9); Pt–C2, 2.113(9); C1–C2, 1.37(2). Selected bond angles (in degrees): N1–Pt–N2, 85.3(3); Pt–C3–C4, 118.9(8); C3–C4–C5, 125.0(1).

phenyl ring is juxtaposed over the *cis*-pyridyl ring, but the methylene group of the dpm ligand removes planarity, which increases the π–π distance for dpm complex **4** compared to that of bpy complex **5**. In the solid state, the π–π distance in **4** is 4.32 Å, whereas in **5**, this distance is only 3.68 Å.⁶

Comparative rates of benzene C–D bond activation by **2** and **3** were studied using reactions with excess C₆D₆ to form [(N~N)Pt(Ph-d₅)(THF)]⁺ (**2-d₅** or **3-d₅**) and free C₆H₅D.

The reaction of **2** and C₆D₆ (0.5 M) occurs with a *k*_{obs} of 9.9(4) × 10⁻⁵ s⁻¹ at 29 °C in CD₂Cl₂ (eq 3). As observed with olefin insertion, benzene C–D bond activation by **2** is almost twice as slow as activation by [(bpy)Pt(Ph)(THF)]⁺ [*k*_{obs} = 1.71(5) × 10⁻⁴ s⁻¹].^{4b}



Complexes [(N~N)Pt(CH₂CH₂Ph)(η²-C₂H₄)]⁺ [N~N = dpm (**4**) or bpy (**5**)] have been identified as the resting states for catalytic ethylene hydrophenylation, and benzene C–H bond activation is likely the catalytic rate-limiting step for complex **3**.^{4b} Relative rates of stoichiometric benzene activation by **4** or **5** to produce ethylbenzene and **2** or **3** are similar to that observed for C₆D₆ activation by **2** and **3**. The dpm complex **4** reacts with benzene (1.5 M) with an observed rate constant of 7.5(3) × 10⁻⁵ s⁻¹ at 54 °C. The reaction using **5** proceeds ~5 times faster with an observed rate constant of ~4 × 10⁻⁴ s⁻¹. Highly accurate integration of ¹H NMR spectra was prevented by coincidental overlap of resonances between **5** and ethylbenzene, and thus, the ratio of rates is approximate.

The rates of the stoichiometric reactions (<90 °C) are significantly reduced for the dpm complex, whether utilizing complex **2** or **4**, versus those of their bpy analogues **3** and **5**, respectively. It was surmised that entropic factors might be important to the overall difference in activation barriers (ΔΔ*G*[‡]) for catalytic ethylene hydrophenylation. The rates of catalytic and stoichiometric reactions were determined over a range of temperatures. Activation parameters for ethylene hydrophenylation by each complex were obtained from Eyring plots (50–100 °C) (Figure 4). Ideally, the rates of catalysis

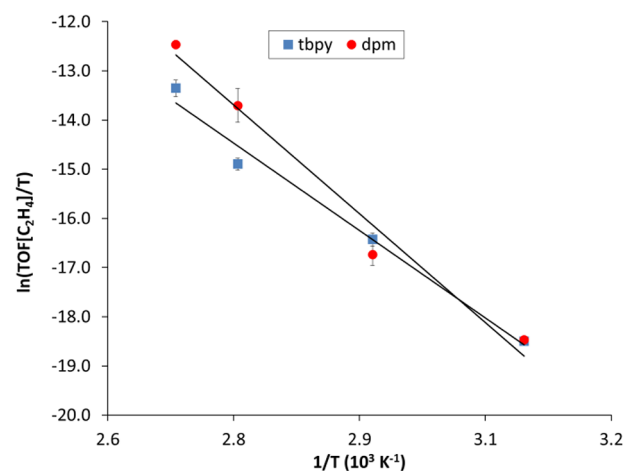


Figure 4. Eyring plots for ethylene hydrophenylation catalyzed by [(N~N)Pt(Ph)(THF)]⁺ [for N~N = bpy (squares), *R*² = 0.98; for N~N = dpm (circles), *R*² = 0.98].

could be determined using *in situ* ¹H NMR spectroscopy. However, significant overlap between the resonances of the catalyst resting state and the alkylbenzene products prevented accurate integration. We chose instead to compare TOFs calculated after reaction times in which catalyst decomposition is negligible (see Figure 2 and Table 2). Using the second-order rate constants for catalyst decomposition, the percent decrease

Table 2. Turnover Frequencies for Ethylene Hydrophenylation (50–100 °C) and Activation Parameters^a

temp (°C)	[(N~N)Pt(Ph)(THF)] ⁺			
	dpm (2)		^t bpy (3)	
	TOF (×10 ⁻⁵ s ⁻¹)	ΔG [‡] _{calcd} (kcal/mol) ^b	TOF (×10 ⁻⁵ s ⁻¹)	ΔG [‡] _{calcd} (kcal/mol) ^b
50 ^c	1.1(3)	27(3)	1.1(1)	27(2)
70 ^c	6.6(5)	27(3)	9(1)	27(2)
90 ^d	140(60)	27(3)	44(5)	27(2)
100 ^e	510(20)	27(3)	210(30)	27(2)
ΔH [‡] (kcal/mol)	29(3)		23(2)	
ΔS [‡] (eu)	6(9)		-11(6)	

^aAt 0.01 mol % catalyst in C₆H₆ with HMB as an internal standard.

^bFree energy of activation calculated using experimental enthalpies and entropies of activation. ^cTOF calculated after 16 h. ^dTOF calculated after 4 h. ^eTOF calculated after 1 h.

in catalyst concentration was determined after 1 h at 100 °C. For catalysis using complex **2**, a decrease in active catalyst concentration is calculated to be <1%. Catalysis with complex **3** is calculated to have ~3.5% catalyst decomposition after 1 h at 100 °C. The negligible degree of catalyst decomposition at 100 °C and the fact that catalyst decomposition at lower temperatures will proceed at slower rates support the use of TO to calculate the TOF for the Eyring plots. The TOF and activation parameters are summarized in Table 2. The values of ΔH[‡] are 29(3) and 23(2) kcal/mol for **2** and **3**, respectively, with a ΔΔH[‡] of 6(4) kcal/mol in favor of the bipyridyl-supported complex **3**. Interestingly, the ΔS[‡] value for **2** [6(9) eu] is positive, while the ΔS[‡] value for **3** [-11(6) eu] is negative and larger in magnitude. Although the deviations for the ΔS[‡] values are relatively large, as is often observed, it is clear that **2** has an entropic advantage over **3**, and the Eyring plot (Figure 4) shows that **2** is a more active catalyst than **3** at ≥90 °C.

Because of the lack of highly accurate integration in ¹H NMR spectra for stoichiometric reactions of **4** and **5** with benzene, activation parameters for stoichiometric C–D bond activation of C₆D₆ by **2** and **3** were obtained from Eyring plots [29–59 °C (Figure 5)]. Enthalpies of activation for C₆D₆ (0.5 M) C–D

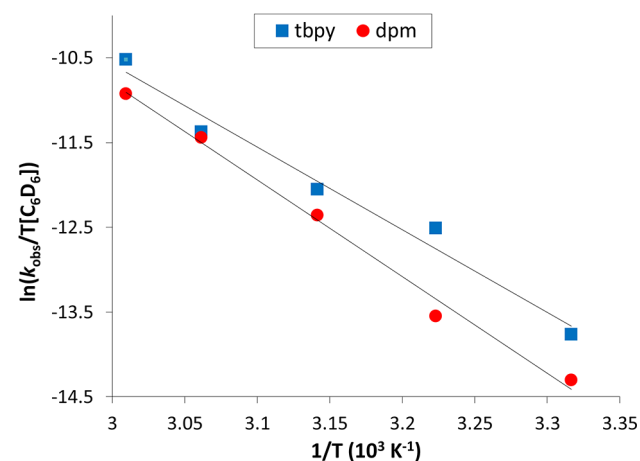


Figure 5. Eyring plots for C₆D₆ C–D bond activation by [(N~N)Pt(Ph)(THF)]⁺ [for N~N = ^tbpy (squares), R² = 0.98; for N~N = dpm (circles), R² = 0.99]. Because of their small values, the deviations are obscured by the size of the data point markers.

bond activation are almost statistically indistinguishable between the complexes with values of 23(2) and 19(2) kcal/mol for **2** and **3**, respectively (Table 3). Similar to the ΔS[‡]

Table 3. Activation Parameters and k_{obs} Values for C₆D₆ C–D Bond Activation at 29–59 °C^a

temp (°C)	[(N~N)Pt(Ph)(THF)] ⁺			
	dpm (2)		^t bpy (3)	
	k _{obs} (×10 ⁻⁴ s ⁻¹)	ΔG [‡] _{calcd} (kcal/mol) ^b	k _{obs} (×10 ⁻⁴ s ⁻¹)	ΔG [‡] _{calcd} (kcal/mol) ^b
29	0.99(4)	23(2)	1.71(4)	22(2)
37	2.00(5)	23(2)	5.7(3)	22(2)
45	6.8(2)	23(2)	9.17(8)	22(2)
54	17.3(4)	23(2)	18.5(5)	22(2)
59	30(2)	23(2)	44(7)	22(2)
ΔH [‡] (kcal/mol)	23(2)		19(2)	
ΔS [‡] (eu)	0(4)		-10(6)	

^aDetermined by ¹H NMR spectroscopy with 0.03 M Pt and 0.5 M C₆D₆ in CD₂Cl₂ with hexamethyldisilane as an internal standard. ^bFree energy of activation calculated using experimental enthalpies and entropies of activation.

values for catalytic ethylene hydrophenylation, **3** suffers a larger entropic penalty, compared to that of **2**, with a ΔS[‡] value of -10(6) eu for the activation of a C–D bond of C₆D₆, while the reaction is almost entropically neutral for **2** [ΔS[‡] = 0(4) eu]. Unfortunately, deviations in ΔS[‡] for C₆D₆ activation are too large to provide a meaningful comparison.

DFT studies were used to compare catalysis with the dpm and ^tbpy complexes. Because [(N~N)Pt(CH₂CH₂Ph)(η²-C₂H₄)]⁺ [N~N = dpm (**4**) or ^tbpy (**5**)] is observed as the catalyst resting state,^{4b} activation parameters for benzene C–H bond activation were calculated relative to these intermediates (full details are provided in the Supporting Information). Given π-arene stacking between a pyridine ring of N~N and the phenyl group of the phenethyl ligand in the crystal structures of [(N~N)Pt(CH₂CH₂Ph)(η²-C₂H₄)]⁺, calculations with and without this interaction in the resting states and transition states were modeled. We focused on C–H oxidative addition of benzene because previous research indicated this to be the preferred pathway for benzene C–H bond activation.^{4b}

For both the dpm and ^tbpy resting states, **4** and **5**, respectively, the nonstacked conformations are calculated to be more favorable at 100 °C (Scheme 2) and were used to calculate activation parameters for benzene C–H bond activation. Table 4 shows calculated activation parameters for the lowest-energy conversions of **4** and **5** to the transition states for benzene C–H bond activation. Consistent with experimental observations, calculated activation parameters for **4** and **5** are similar. At 100 °C, the model predicts complex **4** to have an ~3 kcal/mol advantage over complex **5**. Importantly, DFT calculations indicate a more favorable ΔS[‡] for **4** compared with that for **5**. Given the anticipated limits of such calculations and experimental uncertainties, the DFT calculations are in agreement with experiment.

CONCLUSIONS

In summary, an increase in the chelate size for bis-pyridyl ligands on Pt^{II} catalysts for ethylene hydrophenylation provides an enhancement of the activity and longevity. Using the dpm catalyst precursor **2** provides a TON of ~470, which, to the best of our knowledge, is comparable to the best catalyst for

Scheme 2. Calculated Equilibria (100 °C) between Conformations of Catalyst Resting States with or without π - π Arene Interaction

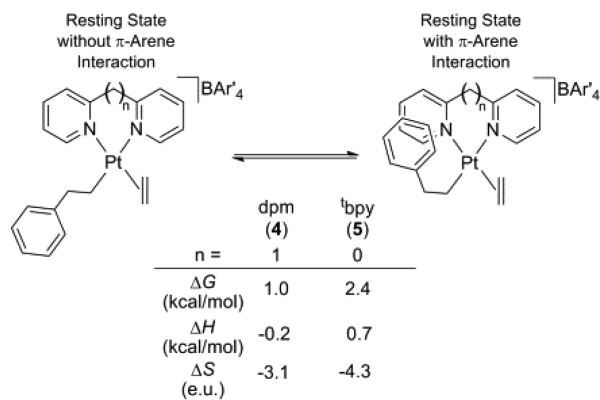


Table 4. Calculated Activation Parameters (100 °C) for Benzene Activation by $[(N\sim N)Pt(CH_2CH_2Ph)(\eta^2-C_2H_4)]^+$

	dpm (4)	^t bpy (5)
ΔG^\ddagger (kcal/mol)	36.8	39.9
ΔH^\ddagger (kcal/mol)	37.0	39.4
ΔS^\ddagger (eu)	0.5	-1.6

ethylene hydrophenylation by a non-acidic pathway. For example, Periana, Goddard, and co-workers have reported that $[Ir(\mu\text{-}acac\text{-}O,O,C_3)(acac\text{-}O,O)(acac\text{-}C_3)]_2$ (**6**) catalyzes ethylene hydrophenylation with a TON of 455 after 3 h at 180 °C, which is, to the best of our knowledge, among the most effective transition metal catalysts for ethylene hydrophenylation.^{4a} Because the conditions for catalysis using **2** and **6** are different, we synthesized and tested **6** for catalytic activity under the conditions used in this study. At 120 °C under 0.1 MPa of ethylene, the iridium-catalyzed reaction (0.01 mol % Ir) yielded 4.0 and 12.9 TO of ethylbenzene after 4 and 16 h, respectively, which corresponds to a TOF of $2.8 \times 10^{-4} \text{ s}^{-1}$. Complex **2** gives a TOF (120 °C) of $1.8 \times 10^{-2} \text{ s}^{-1}$, which is 65 times more active than the Ir catalyst. In addition, we probed the TON using the Ir catalyst **6** at 180 °C using the same catalyst loading that was used in the Pt-catalyzed reactions (i.e., 0.01 mol %). Under these conditions, complex **6** provided an ethylbenzene TON of 161. Thus, complex **2** is among the most active and longest-lived catalysts for the non-acid-catalyzed hydrophenylation of ethylene. Analyses of the elementary steps of the catalytic cycle (e.g., ethylene insertion and benzene C–H bond activation) demonstrate that the larger chelate ring of the dpm ligand provides an entropic advantage compared to that of ^tbpy, which results in increased catalytic activity at elevated temperatures.

EXPERIMENTAL SECTION

General Methods. Unless otherwise noted, all synthetic procedures were performed under anaerobic conditions in a nitrogen-filled glovebox or by using standard Schlenk techniques. Glovebox purity was maintained by periodic nitrogen purges and was monitored by an oxygen analyzer (<15 ppm O₂ for all reactions). Tetrahydrofuran and diethyl ether were dried by distillation from sodium/benzophenone and CaH₂, respectively. *n*-Pentane was distilled over P₂O₅. Methylene chloride and benzene were purified by being passed through a column of activated alumina. Benzene-*d*₆ and

dichloromethane-*d*₂ were used as received and stored under a N₂ atmosphere over 4 Å molecular sieves. ¹H NMR spectra were recorded using a Varian Mercury 300, Unity Innova 500 MHz, or Bruker 800 MHz spectrometer. ¹³C NMR spectra were recorded using a Varian Mercury 300 (operating frequency of 75 MHz), Unity Innova 500 MHz (operating frequency of 125 MHz), or Bruker 800 MHz spectrometer (operating frequency of 201 MHz). All ¹H and ¹³C NMR spectra are referenced against residual proton signals (¹H NMR) or the ¹³C resonances (¹³C NMR) of the deuterated solvents. ¹⁹F NMR (operating frequency of 282 MHz) spectra were obtained on a Varian 300 MHz spectrometer and referenced against an external standard of hexafluorobenzene (δ -164.9). GC/MS was performed using a Shimadzu GCMS-QP2010 Plus system with a 30 m × 0.25 mm SHRXI-SMS column with a 0.25 mm film thickness using negative chemical ionization (NCI), which also allows for simulated electron impact (SEI) ionization, or electron impact (EI) ionization. Ethylene (99.5%) was purchased in a gas cylinder from GTS-Welco and used as received. All other reagents were used as purchased from commercial sources. The preparation, isolation, and characterization of $[Ir(\mu\text{-}acac\text{-}O,O,C_3)(acac\text{-}O,O)(acac\text{-}C_3)]_2$,⁷ $[H(Et_2O)_2][BAR']_4$ [*Ar'* = 3,5-(CF₃)₂C₆H₃],⁸ $[Pt(Ph)_2(Et_2S)]_2$,⁹ 2,2'-dipyridylmethane,¹⁰ $[(^t\text{bpy})Pt(Ph)(THF)][BAR']_4$,^{4b} and $[(^t\text{bpy})Pt(CH_2CH_2Ph)(\eta^2-C_2H_4)][BAR']_4$ ^{4b} have been previously reported.

Computational Methods. All calculations were conducted utilizing Gaussian03.¹¹ The B3LYP¹² functional was employed in conjunction with the Stevens effective core potentials and valence basis sets¹³ augmented by a d polarization function for carbon ($\xi_C = 0.8$) and nitrogen ($\xi_N = 0.8$), viz. CEP-31G(d). Closed-shell (diamagnetic) species were modeled within the restricted Kohn–Sham formalism. All systems were fully optimized without symmetry constraints, and analytic calculations of the energy Hessian were performed to confirm stationary points as minima or transition states and to obtain vibrational frequencies that were used in the calculation of gas-phase free energies at 1 bar and 298.15 K.

Synthesis of (dpm)PtPh₂ (1). To a suspension of $[Pt(Ph)_2(Et_2S)]_2$ (0.35 g, 0.40 mmol) in Et₂O (30 mL) was added 2 equiv of 2,2'-dipyridylmethane (0.14 g, 0.80 mmol). The suspension was stirred at room temperature for ~12 h. The mixture, with a substantial precipitate observed, was reduced *in vacuo*, and hexanes were added (~20 mL). The solution was filtered, and the white precipitate was washed with diethyl ether (2 × 5 mL) and hexanes (2 × 5 mL) and dried under vacuum: isolated 0.35 g (83%); ¹H NMR (800 MHz, CD₂Cl₂) δ 8.45 (d, ³J_{HH} = 6 Hz, 2H, dpm), 7.76 (td, ³J_{HH} = 8 Hz, ⁴J_{HH} = 2 Hz, 2H, dpm), 7.47 (m, 6H, dpm and H^o-Ph), 7.07 (ddd, ³J_{HH} = 8 Hz, ³J_{HH} = 6 Hz, ⁴J_{HH} = 2 Hz, 2H, dpm), 6.90 (t, ³J_{HH} = 8 Hz, 4H, H^m-Ph), 6.77 (t, ³J_{HH} = 7 Hz, 2H, H^p-Ph), 4.74 (br s, 2H, dpm-CH₂); ¹³C NMR (201 MHz, CD₂Cl₂) δ 155.9, 151.9, 145.1, 138.8, 138.1, 127.0, 124.7, 124.2, 121.9 (dpm and Ph aromatic), 47.7 (dpm-CH₂). Anal. Calcd for PtN₂C₂₃H₂₀ (%): C, 53.17; H, 3.89; N, 5.39. Found: C, 52.65; H, 3.98; N, 5.31.

Synthesis of [(dpm)Pt(Ph)(THF)][BAR']₄ (2). A suspension of (dpm)Pt(Ph)₂ (**1**) (0.07 g, 0.1 mmol) in THF (30 mL) was cooled to approximately -70 °C. One equivalent of $[H(Et_2O)_2][BAR']_4$ (0.15 g, 0.10 mmol), dissolved in THF (~10 mL, 303 K), was added. The solution was immediately placed under vacuum, and the volatiles were removed under reduced pressure. The residue was treated with *n*-pentane (~2

mL), which was then removed under vacuum to afford a fluffy blue-green solid. The solid was dried *in vacuo*: isolated 0.17 g (90%); ^1H NMR (500 MHz, CD_2Cl_2) δ 8.47 (t, $^3J_{\text{HH}} = 6$ Hz, 2H, dpm), 7.92 (td, $^3J_{\text{HH}} = 8$ Hz, $^4J_{\text{HH}} = 2$ Hz, 1H, dpm), 7.80 (td, $^3J_{\text{HH}} = 8$ Hz, $^4J_{\text{HH}} = 2$ Hz, 1H, dpm), 7.73 (s, 8H, $\text{H}^{\text{o-}}\text{Ar}'$), 7.62 (d, $^3J_{\text{HH}} = 8$ Hz, 1H, dpm), 7.56 (s, 4H, $\text{H}^{\text{p-}}\text{Ar}'$), 7.48 (overlapping m, 2H, dpm), 7.37 (dd, $^3J_{\text{HH}} = 8$ Hz, $^4J_{\text{HH}} = 1$ Hz, 2H, $\text{H}^{\text{o-}}\text{Ph}$), 7.09 (t, $^3J_{\text{HH}} = 8$ Hz, 2H, $\text{H}^{\text{m-}}\text{Ph}$), 7.04 (ddd, $^3J_{\text{HH}} = 8$ Hz, $^3J_{\text{HH}} = 6$ Hz, $^4J_{\text{HH}} = 2$ Hz, 1H, dpm) 6.98 (t, $^3J_{\text{HH}} = 7$ Hz, 1H, $\text{H}^{\text{p-}}\text{Ph}$), 4.64 (v br s, 2H, dpm- CH_2), 4.05 (s, 4H, α -THF), 1.78 (s, 4H, β -THF); ^{13}C NMR (75 MHz, CD_2Cl_2) δ 162.3 (q, Ar', $^1J_{\text{BCipso}} = 49$ Hz), 156.7, 154.6, 153.7, 149.8, 140.8, 140.3, 136.5, 135.2 (Ar'), 129.4 (q, *m*-Ar', $^2J_{\text{CF}} = 32$ Hz), 128.7, 128.2, 126.4, 125.9, 125.5, 125.4, 125.2 (dpm and Ph aromatic), 125.0 (q, CF_3 -Ar', $^1J_{\text{CF}} = 272$ Hz), 117.9 (Ar'), 77.4 (α -THF), 47.4 (dpm- CH_2), 24.9 (β -THF); ^{19}F NMR (282 MHz, CD_2Cl_2) δ -63.1 (s, CF_3 -Ar'). Anal. Calcd for $\text{PtN}_2\text{OBF}_2\text{C}_{53}\text{H}_{35}$ (%): C, 46.20; H, 2.57; N, 2.03. Found: C, 45.96; H, 2.44; N, 2.13.

Synthesis of $[(\text{dpm})\text{Pt}(\text{CH}_2\text{CH}_2\text{Ph})(\eta^2\text{-C}_2\text{H}_4)][\text{BAR}'_4]$ (4).

A solution of **2** (0.042 g, 0.031 mmol) in CD_2Cl_2 (20 mL) was transferred to a stainless steel reactor. The reactor was then pressurized with 3.5 bar of C_2H_4 . The reaction mixture was stirred for 6 h. The volatiles were removed under vacuum. The residue was treated with *n*-pentane (~2 mL), which was then removed under vacuum to afford a fluffy solid. The solid was then dried *in vacuo*: isolated 0.037 g (89%); ^1H NMR (500 MHz, CD_2Cl_2) δ 8.62 (d, $^3J_{\text{HH}} = 6$ Hz, 1H, dpm), 8.19 (d, $^3J_{\text{HH}} = 6$ Hz, 1H, dpm), 8.01 (td, $^3J_{\text{HH}} = 8$ Hz, $^4J_{\text{HH}} = 2$ Hz, 1H, dpm), 7.85 (td, $^3J_{\text{HH}} = 8$ Hz, $^4J_{\text{HH}} = 2$ Hz, 1H, dpm), 7.74 (s, 8H, $\text{H}^{\text{o-}}\text{Ar}'$), 7.62–7.45 (m, 7H, $\text{H}^{\text{p-}}\text{Ar}'$, $\text{H}^{\text{o-}}\text{Ph}$ and dpm), 7.40 (ddd, $^3J_{\text{HH}} = 8$ Hz, $^3J_{\text{HH}} = 6$ Hz, $^4J_{\text{HH}} = 2$ Hz, 1H, dpm), 7.18–7.04 (m, 3H, $\text{H}^{\text{m-}}\text{Ph}$ and $\text{H}^{\text{p-}}\text{Ph}$), 6.99–6.93 (m, 2H, dpm), 4.15–3.91 (m, 6H, dpm- CH_2 and C_2H_4), 2.25 (t, $^3J_{\text{HH}} = 7$ Hz, 2H, $-\text{CH}_2\text{CH}_2\text{Ph}$), 1.45–1.23 (m, 2H, $-\text{CH}_2\text{CH}_2\text{Ph}$); ^{13}C NMR (125 MHz, CD_2Cl_2) δ 162.2 (q, Ar', $^1J_{\text{BCipso}} = 49$ Hz), 154.7, 153.0, 149.6, 147.8, 143.6, 142.3, 141.2, 135.2 (Ar'), 129.3 (q, *m*-Ar', $^2J_{\text{CF}} = 32$ Hz), 129.0, 128.3, 127.0, 126.7, 126.4, 126.1, 125.0 (q, Ar', $^1J_{\text{CF}} = 272$ Hz), 117.9 (Ar'), 100.9 (dpm and Ph aromatic), 73.0 (s with Pt satellites, $^1J_{\text{PtC}} = 210$ Hz, C_2H_4), 46.2 (dpm- CH_2), 36.9 ($-\text{CH}_2\text{CH}_2\text{Ph}$), 15.3 ($-\text{CH}_2\text{CH}_2\text{Ph}$); ^{19}F NMR (282 MHz, CD_2Cl_2) δ -63.1 (s, CF_3 -Ar'). Anal. Calcd for $\text{PtN}_2\text{BF}_2\text{C}_{53}\text{H}_{35}$ (%): C, 46.74; H, 2.60; N, 2.06. Found: C, 46.35; H, 2.73; N, 2.10.

Catalytic Olefin Hydrophenylation. A representative catalytic reaction is described. $[(\text{dpm})\text{Pt}(\text{Ph})(\text{THF})][\text{BAR}'_4]$ (**2**) (0.019 g, 0.013 mmol) was dissolved in 12.0 mL of benzene containing 0.01 mol % hexamethylbenzene (HMB) relative to benzene as an internal standard. The reaction mixture was placed in a stainless steel pressure reactor, charged with ethylene (0.1 MPa), pressurized to a total of 0.8 MPa with N_2 , and heated to 100 °C. After a given time period, the reaction mixture was allowed to cool to room temperature and was analyzed by GC/MS. Peak areas of the products and the internal standard were used to calculate product yields. Ethylbenzene production was quantified using linear regression analysis of gas chromatograms of standard samples. A set of five known standards were prepared consisting of 2:1, 4:1, 6:1, 8:1, and 10:1 molar ratios of ethylbenzene to HMB in benzene. A plot of the peak area ratios versus molar ratios gave a regression line. For the GC/MS system, the slope and correlation coefficient (R^2) for ethylbenzene were 0.68 and 0.99, respectively. Identical procedures were used to quantify the

production of styrene, 1,3-diethylbenzene, 1,4-diethylbenzene, and 1,2-diethylbenzene. The slope and correlation coefficients (R^2) for these species are 0.51 and 0.99, 0.52 and 0.99, 0.53 and 0.99, and 0.55 and 0.99, respectively.

Determination of the Catalyst Resting State for Ethylene Hydrophenylation Using Complex 2. Complex **2** (0.02 g, 0.01 mmol) was weighed into a J-Young NMR tube and dissolved in C_6D_6 (0.4 mL). The tube was then pressurized with 0.1 MPa of ethylene and placed in a temperature-equilibrated NMR probe (90 °C setting). The actual temperature of the probe (89 °C) was determined using a solution of 80% ethylene glycol in $\text{DMSO}-d_6$.¹⁴ Spectra were collected every 15 min for 4 h with eight scans and a 5.0 s pulse delay. Beginning with the initial spectrum, the only observable Pt species in solution was $[(\text{dpm})\text{Pt}(\text{CH}_2\text{CH}_2\text{Ph})(\eta^2\text{-C}_2\text{H}_4)]\text{[BAR}'_4]$.

Kinetics of Ethylene Insertion. A representative kinetic experiment is described. Complex **2** (0.057 g, 0.041 mmol) and hexamethyldisilane (HMDS, 2.0 μL as an internal standard) were dissolved in 1.3 mL of CD_2Cl_2 . The solution was then divided (0.4 mL for each sample) and added to three high-pressure NMR tubes. Each tube was pressurized with 0.4 MPa of ethylene and placed into a temperature-equilibrated (25 °C setting) NMR probe. The actual temperature of the probe (23 °C) was determined using a sample of methanol- d_4 .¹⁵ Kinetic runs were performed in triplicate. The concentration of ethylene in solution was determined by integration against the internal standard, HMDS. ^1H NMR spectra were collected every 1 min with four scans and a 5.0 s pulse delay. The product peaks were integrated against that of HMDS, and from a plot of $\ln(1 - [4]_t/[2]_0)$ versus time (seconds), the rate constants were extracted. The rate of formation of **4** from complex **2**, in the presence of 0.5 M C_2H_4 , was $8.4(9) \times 10^{-4} \text{ s}^{-1}$ with a correlation coefficient (R^2) of 0.99 for each plot.

Kinetics of Benzene- d_6 C–D Bond Activation. A representative kinetic experiment is described. Complex **2** (0.064 g, 0.046 mmol) and hexamethyldisilane (HMDS, 2.0 μL as an internal standard) were dissolved in 1.2 mL of CD_2Cl_2 . The solution was then divided (0.375 mL for each sample) and added to three NMR tubes. To each tube was added C_6D_6 (0.019 mL, 0.21 mmol). The tube was placed into a temperature-equilibrated (30 °C setting) NMR probe. The actual temperature of the probe (29 °C) was determined using a solution of 80% ethylene glycol in $\text{DMSO}-d_6$.¹⁴ Kinetic runs were performed in triplicate. ^1H NMR spectra were collected every 10 min with eight scans and a 5.0 s pulse delay. Resonances for complex **2** were integrated against that of the internal standard, HMDS, and from a plot of $\ln([2]_t)$ versus time (seconds), the rate constants were extracted. The rate of formation of complex **2-d**₅ and $\text{C}_6\text{H}_5\text{D}$ in the presence of 0.5 M C_6D_6 was $9.9(4) \times 10^{-5} \text{ s}^{-1}$ with a correlation coefficient (R^2) of 0.99 for each plot.

Substrate Concentration Corrections for the Determination of Catalytic Activation Parameters. Catalysis with complexes **2** and **3** was performed under conditions that are inverse first-order in ethylene concentration. Therefore, for the Eyring analysis, the observed rate constants were multiplied by the concentration of ethylene. The ethylene concentration under catalytic conditions was simulated by sparging a sample of C_6D_6 in a J-Young NMR tube with ethylene and pressurizing it according to the preparation of catalytic reaction mixtures. The concentration of ethylene was then determined in triplicate

by integration of the ethylene resonance versus the internal standard, HMDS, at 90 °C.

Substrate Concentration Corrections for the Determination of C₆D₆ Activation Parameters. The reactions with C₆D₆ and complexes 2 and 3 were performed under conditions that are first-order in the concentration of C₆D₆. Therefore, for Eyring analysis, the observed rate constants were divided by the concentration of C₆D₆.

Crystal Structure of [(dpm)Pt(CH₂CH₂Ph)(η²-C₂H₄)]-[BAR'₄] **(3). X-ray intensities were measured on a Bruker Apex II Kappa Duo CCD diffractometer (Mo Kα radiation, λ = 0.71073 Å) at 120 K; 2358 frames were collected up to 2θ of 48.9°. Intensities were corrected for absorption by applying Bruker SADABS.¹⁶ The structure was determined using direct methods and standard difference map techniques and was refined by full-matrix least-squares procedures on F² with SHELXTL (version 6.14).¹⁷ All non-hydrogen atoms were refined anisotropically. Hydrogen atoms were included in calculated positions and were refined using a riding model: C₅₃H₃₅BF₂₄N₂Pt, M_w = 1361.73, monoclinic, space group P2(1)/c, a = 18.556(2) Å, b = 17.006(2) Å, c = 17.621(2) Å, β = 103.297(2)°, V = 5411.3(9) Å³, Z = 4, ρ_{calcd} = 1.671 g cm⁻³. Of 59891 measured reflections, 8865 were independent (R_{int} = 0.0627); 746 parameters, R1 = 0.0562 [for reflections with I > 2σ(I)], wR2 = 0.1707 (for all reflections). CCDC-916579 contains the supplementary crystallographic data for this paper, which can be obtained free of charge from the Cambridge Crystallographic Data Centre (http://www.ccdc.cam.ac.uk/data_request/cif).**

■ ASSOCIATED CONTENT

● Supporting Information

Full computational study with discussion. This material is available free of charge via the Internet at <http://pubs.acs.org>.

■ AUTHOR INFORMATION

Corresponding Author

*E-mail: tbg7h@virginia.edu (T.B.G.) or t@unt.edu (T.R.C.).

Notes

The authors declare no competing financial interest.

■ ACKNOWLEDGMENTS

T.B.G. and T.R.C. acknowledge The Office of Basic Energy Sciences, U.S. Department of Energy, for support of this work (DE-SC0000776 and DE-FG02-03ER15387) and the National Science Foundation for purchase of an X-ray diffractometer (CHE-1126602).

■ REFERENCES

- (1) (a) Olah, G. A.; Molnar, A. *Hydrocarbon Chemistry*; Wiley-Interscience: New York, 1995. (b) Roberts, R. M.; Khalaf, A. A. *Friedel-Crafts Alkylation Chemistry: A Century of Discovery*; Marcel Dekker, Inc.: New York, 1984. (c) Čejka, J.; Wichterlová, B. *Catal. Rev.* **2002**, *44*, 375–421. (d) Kocal, J. A.; Vora, B. V.; Imai, T. *Appl. Catal., A* **2001**, *221*, 295–301. (e) Perego, C.; Ingallina, P. *Green Chem.* **2004**, *6*, 274–279.
- (2) (a) Goj, L. A.; Gunnoe, T. B. *Curr. Org. Chem.* **2005**, *9*, 671–685. (b) Andreatta, J. R.; McKeown, B. A.; Gunnoe, T. B. *J. Organomet. Chem.* **2011**, *696*, 305–315. (c) Foley, N. A.; Lee, J. P.; Ke, Z.; Gunnoe, T. B.; Cundari, T. R. *Acc. Chem. Res.* **2009**, *42*, 585–597. (d) Luedtke, A. T.; Goldberg, K. I. *Angew. Chem., Int. Ed.* **2008**, *47*, 7694–7696.
- (3) (a) Yoshikai, N. *Synlett* **2011**, *2011*, 1047–1051. (b) Harada, H.; Thalji, R. K.; Bergman, R. G.; Ellman, J. A. *J. Org. Chem.* **2008**, *73*,

6772–6779. (c) Colby, D. A.; Bergman, R. G.; Ellman, J. A. *Chem. Rev.* **2010**, *110*, 624–655. (d) Dyker, G.; Muth, E.; Hashmi, A. S. K.; Ding, L. *Adv. Synth. Catal.* **2003**, *345*, 1247–1252. (e) Ritleng, V.; Sirlin, C.; Pfeffer, M. *Chem. Rev.* **2002**, *102*, 1731–1769. (f) Kakiuchi, F.; Murai, S. *Acc. Chem. Res.* **2002**, *35*, 826–834.

(4) (a) Matsumoto, T.; Taube, D. J.; Periana, R. A.; Taube, H.; Yoshida, H. *J. Am. Chem. Soc.* **2000**, *122*, 7414–7415. (b) McKeown, B. A.; Gonzalez, H. E.; Friedfeld, M. R.; Gunnoe, T. B.; Cundari, T. R.; Sabat, M. *J. Am. Chem. Soc.* **2011**, *133*, 19131–19152. (c) McKeown, B. A.; Foley, N. A.; Lee, J. P.; Gunnoe, T. B. *Organometallics* **2008**, *27*, 4031–4033.

(5) Zhang, F. B.; Kirby, C. W.; Hairsine, D. W.; Jennings, M. C.; Puddephatt, R. J. *J. Am. Chem. Soc.* **2005**, *127*, 14196–14197.

(6) Distance measured from the Ph centroid to the *cis*-pyridyl centroid using the graphical program ChemCraft and atom coordinates from single-crystal X-ray diffraction.

(7) Bennett, M. A.; Mitchell, T. R. B. *Inorg. Chem.* **1976**, *15*, 2936–2938.

(8) Brookhart, M.; Grant, B.; Volpe, A. F. *Organometallics* **2002**, *21*, 3920–3922.

(9) Steele, B. R.; Vrieze, K. *Transition Met. Chem. (Dordrecht, Neth.)* **1977**, *2*, 140–144.

(10) Canty, A.; Minchin, N. *Aust. J. Chem.* **1986**, *39*, 1063–1069.

(11) de Graaf, W.; Boersma, J.; Smeets, W. J. J.; Spek, A. L.; van Koten, G. *Organometallics* **1989**, *8*, 2907–2917.

(12) (a) Becke, A. D. *J. Chem. Phys.* **1993**, *98*, 1372–1377. (b) Lee, C.; Yang, W.; Parr, R. G. *Phys. Rev.* **1998**, *B37*, 785–789.

(13) Stevens, W. J.; Krauss, M.; Basch, H.; Jasien, P. G. *Can. J. Chem.* **1992**, *70*, 610–613.

(14) The temperature was verified using the following equation provided by the Bruker Instruments, Inc., VT-Calibration Manual: $T(K) = (4.218 - X)/0.009132$, where X is the parts per million of OH – the parts per million of CH₂.

(15) The temperature was verified using the following equation provided by experimental data from the University of Nebraska (2001): $T(K) = -23.1902x^2 - 31.1062x + 399.081$, where x is the parts per million of OD vs the parts per million of CD₃.

(16) *Bruker Apex 2 User Manual*; Bruker AXS Inc.: Madison, WI, 2010.

(17) Sheldrick, G. *Acta Crystallogr.* **2008**, *A64*, 112–122.